A&A manuscript no.
(will be inserted by hand later)

Your thesaurus codes are:
(03.20.1; 11.17.4 Q 2237+0305; 12.07.1)

ASTRONOMY AND ASTROPHYSICS

Three photometric methods tested on ground-based data of Q 2237+0305⋆

I. Burud[1,2], R. Stabell[2,3], P. Magain[1,⋆⋆], F. Courbin[1,4], R. Østensen[1,5], S. Refsdal[3,6], M. Remy[1], J. Teuber[3]

[1] Institut d'Astrophysique, Université de Liège, Avenue de Cointe 5, B–4000 Liège, Belgium
[2] Institute of Theoretical Astrophysics, University of Oslo, Pb. 1029 Blindern, 0315 Oslo, Norway
[3] Centre for Advanced Study, Drammensveien 78, N-0271 Oslo, Norway
[4] URA 173 CNRS-DAEC, Observatoire de Paris, F–92195 Meudon Principal Cédex, France
[5] Department of Physics, University of Tromsø, N-9037 Tromsø, Norway
[6] Hamburger Sternwarte, Gojenbergsweg 112, D-21029 Hamburg, Germany

Receiveved 01 July, 1998; Accepted 25 August ,1998

Abstract. The Einstein Cross, Q 2237+0305, has been photometrically observed in four bands on two successive nights at NOT (La Palma, Spain) in October 1995. Three independent algorithms have been used to analyse the data: an automatic image decomposition technique, a CLEAN algorithm and the new MCS deconvolution code. The photometric and astrometric results obtained with the three methods are presented. No photometric variations were found in the four quasar images. Comparison of the photometry from the three techniques shows that both systematic and random errors affect each method. When the seeing is worse than 1.″0, the errors from the automatic image decomposition technique and the Clean algorithm tend to be large (0.04-0.1 magnitudes) while the deconvolution code still gives accurate results (1σ error below 0.04) even for frames with seeing as bad as 1.″7.

Reddening is observed in the quasar images and is found to be compatible with either extinction from the lensing galaxy or colour dependent microlensing.

The photometric accuracy depends on the light distribution used to model the lensing galaxy. In particular, using a numerical galaxy model, as done with the MCS algorithm, makes the method less seeing dependent. Another advantage of using a numerical model is that eventual non-homogeneous structures in the galaxy can be modeled.

Finally, we propose an observational strategy for a future photometric monitoring of the Einstein Cross.

Key words: quasars: individual: Q 2237+0305 - gravitational lensing - Techniques: image processing

Send offprint requests to: I. Burud, Liège address. Email: burud@astro.ulg.ac.be

⋆ Based on observations obtained at NOT, La Palma.

⋆⋆ Maître de Recherches au Fonds National Belge de la Recherche Scientifique

1. Introduction

The gravitational lens system Q 2237+0305, known as the Einstein Cross, is one of the most promising objects to observe intensity variations due to microlensing of quasar images. The object, discovered by Huchra et al. (1985), consists of four images of the same quasar at $z = 1.69$ lensed by a foreground spiral galaxy at $z = 0.04$. The maximum angular separation of the components is about 1.″8. Due to the proximity of the lens and the high degree of symmetry of the system, the time delays between the images are of the order of one day. Intrinsic variations of the source therefore show up almost simultaneously in all four quasar images, hence making them easy to distinguish from microlensing effects. This system with a low-redshift lens is an ideal case for studying microlensing effects, since the light paths to the different QSO images pass through the bulge of the galaxy, hence increasing the probability of gravitational influence by single stars (Chang & Refsdal 1979, Paczynski 1986, Kayser et al. 1986, Kayser & Refsdal 1989). In addition we note that the angular size of the Einstein ring for a given lens mass is larger than for systems with higher lens redshifts.

However, detecting faint intensity variations in multiply imaged QSOs requires very accurate photometry. For most gravitationally lensed QSOs, this is not a straightforward task, Q 2237+0305 being one of the most complicated cases. Given the blending of the QSO images, aperture photometry is excluded and profile fitting photometry is not trivial. Moreover, since the foreground galaxy has a sharp nucleus creating a non-uniform and fast-varying background, the light distribution of the lensing galaxy has to be modeled carefully.

Several methods and algorithms have been developed to perform PSF photometry of blended sources and more specific codes have been developed to treat the Einstein Cross. We compare in the following, three of these meth-

ods (described in section 3): an automatic PSF fitting technique (M. Remy 1996, hereafter the Fitting method), an interactive CLEAN algorithm (R. Østensen 1994), and a deconvolution method (P. Magain, F. Courbin & S. Sohy 1998, hereafter MCS).

For this purpose, numerous images of the Einstein Cross were taken on two successive nights at the Nordic Optical Telescope (NOT) at La Palma, Canary Islands (Spain). A homogeneous set of data taken over a short time scale with a good temporal sampling was obtained. No physical intensity variations were likely to be detected in the object during such a short period so that the data set is very well suited for performing photometric tests. For each method, we measured the photometric robustness with respect to the seeing variations in optical B, V, R, I-bands.

If we detected real variations during the two nights, we would have had the chance to observe either a high amplification microlensing event (if the variation had occurred in one image only) or an intrinsic fluctuation in the quasar itself, which could have led to the determination of the time delay for this system.

2. Observations

The observations took place at the NOT on the nights of October 10 and 11, 1995. We used the CCD camera BroCam 1 equipped with a thinned backside illuminated TEK 1024 CCD with a conversion factor of $q = 1.7e^{-}ADU^{-1}$, a readout noise of $6.5e^{-}$ and a pixel size of $0\farcs176$. Sequences of exposures were obtained through the filters B, V, R and I (in this order). The total number of frames obtained of the Einstein Cross in each band, as well as the total exposure time and the mean seeing value are summarized in Table 1. The seeing of the frames varied between $0\farcs6$ and $1\farcs7$.

Table 1. Log of observations of the Einstein Cross from the 10^{th} and 11^{th} of October 1995. The first two lines show the total number of frames in each band. The next two lines give the total exposure time and the mean seeing value.

	B	**V**	**R**	**I**
1^{st} **night**	6	9	8	9
2^{nd} **night**	7	9	7	9
total exp. time	3400 s	4100 s	3100 s	3750 s
Mean seeing	$0\farcs94$	$0\farcs94$	$0\farcs86$	$0\farcs82$

Bias subtraction, flat-field correction (sky-flats) and cosmic ray removal were applied to the raw data using the ESO MIDAS routines. In order to model and subtract low frequency sky variations across the frames, bi-quadratic polynomial surfaces were fitted to a well sampled grid of empty regions in each individual frame.

3. Photometric methods

3.1. The Fitting method

A profile fitting method has been developed in the MIDAS environment by M. Remy (1996) in order to obtain accurate photometric measurements of multiply imaged quasars. This method has already been applied to other lensed systems, (e.g., H1413+117, the Cloverleaf, Østensen et al. 1997). Unlike the Einstein Cross, the Cloverleaf system does not suffer from the contamination of a bright and complicated foreground lens, and is therefore much easier to study.

In the present case, the magnitudes of the quasar images were determined by fitting simultaneously numerical PSFs to the point sources, and a de Vaucouleurs function ($R^{-1/4}$) to the galaxy. An additional Moffat profile was also fitted (still simultaneously) in order to model the point-like galaxy nucleus. All the parameters were adjusted by the program, using a χ^2 minimization. The intensity and positions for the four numerical PSFs and for the Moffat profile were determined as well as the shape and rotational parameters of the Moffat and the de Vaucouleurs model.

The technique was tested in different ways on our images. First, the fit was performed with all the parameters free on the whole data set. From these results, we calculated the mean positions of the QSO components and the galaxy nucleus. Then we ran the program with the position parameters fixed relative to component A. Furthermore, a galaxy model with fixed shape parameters was obtained by extracting the galaxy from the best result in each band. It was then convolved to the respective seeing of each individual frame. Another fit was performed with a fixed galaxy model centered on the nucleus, i.e. only its intensity was left as free parameter. The advantage of freezing the relative positions of the QSO images and the galaxy model is to minimize the number of free parameters in the fit. On the other hand, if the positions and the galaxy model are not accurate, we may introduce systematic errors. In the present case, the best χ^2 fit was obtained with all the positions fixed relative to component A, and a de Vaucouleurs profile with fixed parameters. Section 4.1 presents the results obtained in this way.

3.2. A CLEAN algorithm

A program for CLEAN photometry of overlapping point sources has been developed by R. Østensen (1994), and implemented using IDL. This program, called XECClean, has been specifically designed to perform photometry on the Einstein Cross and has been applied to the NOT monitoring data of the object (Østensen et al. 1996). As for the Fitting method, the programme has also been used on the monitoring data of H1413+117 (Østensen et al. 1997).

XECClean applies a semi-analytical PSF-profile fitting procedure adapted from the DAOPHOT package (Stetson 1987), and "deconvolves" the images using an interactive CLEAN algorithm (e.g., Teuber 1993). A PSF is successively fitted and removed from each QSO image until a first convergence of the parameters is reached. Once the point sources are removed, a de Vaucouleurs profile with fixed shape parameters is centered on the galaxy nucleus and convolved to the seeing of each frame. This model is fitted to the lensing galaxy and subtracted from the image. Then the quasar components and the galaxy are iteratively restored, fitted again, and removed until convergence is reached. This is repeated as many times as necessary for obtaining satisfactory residuals for each frame.

3.3. The MCS deconvolution algorithm

A new deconvolution method has been developed by Magain et al. (1998). Contrary to traditional methods of deconvolution, this algorithm allows not only a significant increase in the spatial resolution of the images, but also to perform accurate photometric and astrometric measurements on the deconvolved frames.

The algorithm is based on the principle that sampled data cannot be fully deconvolved without recovering Fourier frequencies higher than the Nyquist frequency, and violate the sampling theorem. A sampled image should therefore not be deconvolved by the total PSF but by a narrower function chosen so that the resolution of the deconvolved image is compatible with the adopted sampling.

The image is decomposed into a sum of point sources plus a diffuse background. The background is constrained to be smoothed on the length scale of the final resolution, chosen by the user. The best model image is computed by minimizing the χ^2 using a modified version of the conjugate gradient method (Press et al. 1989). Positions and intensities of the point sources as well as the image of the deconvolved background are given as output of the deconvolution procedure.

Successful results have already been obtained on several gravitational lens systems (e.g., Courbin et al. 1998a, 1998b). In the present case, we chose the pixel size of the deconvolved frame to be half the one in the original data, $0\farcs176/2 = 0\farcs088$. Furthermore, we adopted for the deconvolved point source a Gaussian profile with a FWHM of 3 (small) pixels, which allows us to reach a final resolution of $0\farcs26$. The deconvolution of our images was performed in two steps. First, the frames in a given filter were averaged, giving a deep image of the object. This image was deconvolved in order to obtain an accurate numerical model of the lensing galaxy. Since the galaxy profile varies sharply in the vicinity of the nucleus, we applied a variable smoothing parameter λ across the field, in order to avoid local over- or underfitting of the data (see Magain et al. 1998). Since the nucleus-shape is close to that of a point

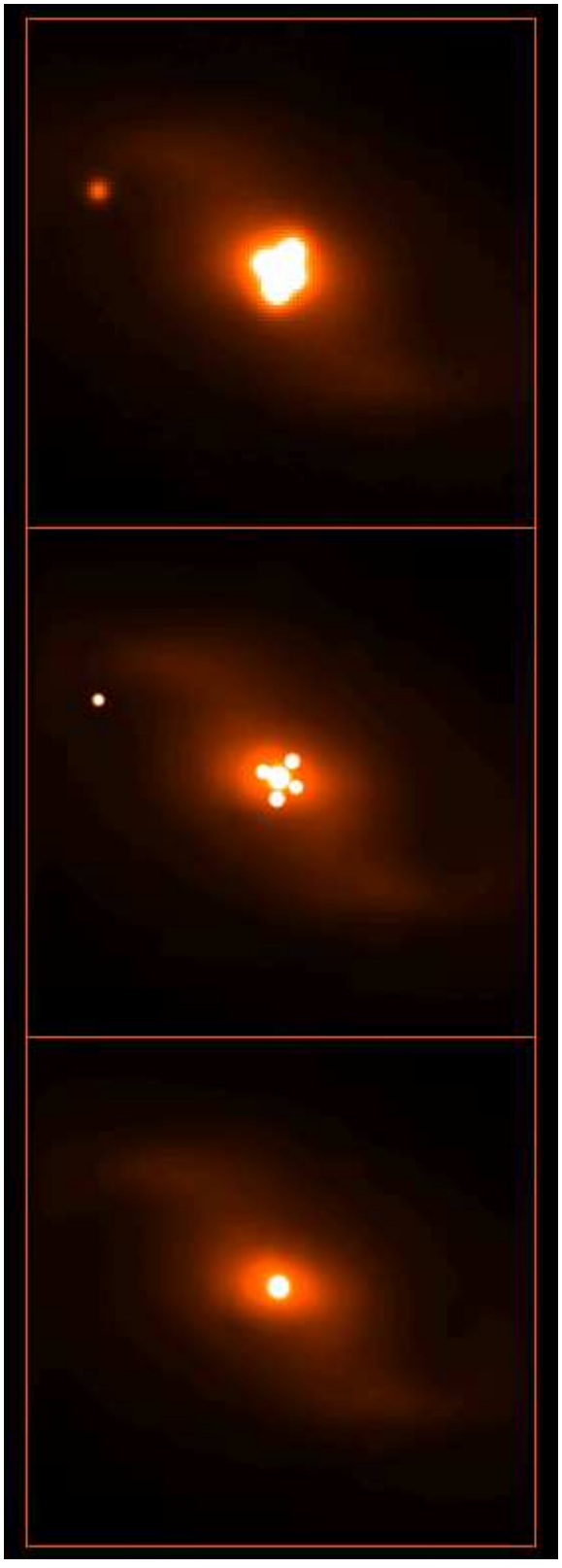

Fig. 1. [*Top*]: Stack of 12 R band frames with a seeing of $\sim 0\farcs8$. [*Middle*]: Deconvolved frame using the MCS algorithm. The resolution is now $0\farcs26$. [*Bottom*]: Deconvolved numerical galaxy model. All the images are $\sim 22''$ on a side, North is up and East is to the left.

source, but not exactly, we added a quasi-point-source described by a Moffat profile, for the nucleus. Its intensity, position and shape parameters were all determined by the deconvolution program.

Fig. 1 presents the result obtained from the stack of our R-band frames. The top and the middle panels show the observed and the deconvolved frame respectively, and the bottom panel displays the numerical galaxy model obtained by the algorithm. Both the point sources (quasar components and foreground star) and the lensing galaxy appear clearly without any deconvolution artifacts. The separation of the point sources from the background allows one to study the deflector alone, without the disturbing light from the quasar's images. We could in this way determine an accurate numerical model for the lensing galaxy, that can be used for future photometric monitoring.

After a numerical model of the galaxy had been obtained in each band, it was used as a fixed background for the deconvolution of the individual frames. Only a multiplicative factor and an additive term were applied in order to correct for different exposure times (e.g., shutter effects) and varying sky-levels. The frames were deconvolved both separately and simultaneously. The advantage of simultaneous deconvolution is that the solution is compatible with all the images considered. The intensities of the point sources are allowed to converge to different values from one frame to another so that intrinsic variations in the object can be detected, while the positions of the point sources are constrained by all the images used.

4. Results

4.1. Photometric results

Our photometric magnitudes are calibrated by means of Yee's (1988) reference star, using the transformation equations and revised values given by Corrigan et al. (1991). No significant intensity variation was detected on the data during the two nights of observation. Therefore a mean magnitude could be calculated for each QSO image and a 1σ error for the results obtained with each method. These values, as well as the calculated error on the mean magnitude, are shown in Tables 2, 3, 4, and 5 for the B,V, R, I filters respectively. The standard deviation of the mean σ_{mean} was calculated in order to give an estimate of the error for each QSO image in each filter and is simply the standard deviation for all the frames divided by the square root of the number of frames used.

In order to make sure that the magnitudes of the QSO images did not vary during the run, we looked for possible systematic correlations between the results of the different methods. No such correlation was found. Therefore we can safely assume that the QSO images did not vary and we can use the data set to compare the three algorithms.

For the Fitting method and the CLEAN algorithm, the photometry depends on the seeing of the frame, i.e.,

Table 2. B-band photometric results: mean magnitude and standard deviations

	Fitting	**Clean**	**Deconv**
A	17.612 ± 0.025	17.626 ± 0.033	17.655 ± 0.029
σ_{mean}	± 0.007	± 0.009	± 0.008
B	17.754 ± 0.040	17.741 ± 0.030	17.754 ± 0.023
σ_{mean}	± 0.011	± 0.008	± 0.006
C	18.937 ± 0.076	18.881 ± 0.073	18.885 ± 0.040
σ_{mean}	± 0.021	± 0.020	± 0.011
D	19.155 ± 0.034	19.111 ± 0.121	19.220 ± 0.040
σ_{mean}	± 0.009	± 0.033	0.011

Table 3. V-band photometric results: mean magnitude and standard deviations. We have removed one of the frames with a FWHM=1.″63 in the results from the Fitting and CLEAN algorithms.

	Fitting	**Clean**	**Deconv**
A	17.257 ± 0.018	17.278 ± 0.019	17.276 ± 0.016
σ_{mean}	± 0.004	± 0.004	± 0.004
B	17.414 ± 0.014	17.428 ± 0.022	17.425 ± 0.015
σ_{mean}	± 0.003	± 0.009	± 0.004
C	18.531 ± 0.062	18.389 ± 0.028	18.415 ± 0.035
σ_{mean}	± 0.015	± 0.009	± 0.008
D	18.801 ± 0.070	18.734 ± 0.075	18.704 ± 0.031
σ_{mean}	± 0.017	± 0.022	± 0.007

Table 4. R-band photometric results: mean magnitude and standard deviations. We have removed one of the frames with a FWHM=1.″48 in the result from the Fitting technique.

	Fitting	**Clean**	**Deconv**
A	17.078 ± 0.020	17.093 ± 0.014	17.106 ± 0.021
σ_{mean}	± 0.006	± 0.004	± 0.005
B	17.262 ± 0.027	17.274 ± 0.014	17.291 ± 0.023
σ_{mean}	± 0.008	± 0.004	± 0.006
C	18.227 ± 0.030	18.109 ± 0.032	18.093 ± 0.042
σ_{mean}	± 0.009	± 0.008	± 0.011
D	18.522 ± 0.048	18.441 ± 0.039	18.378 ± 0.032
σ_{mean}	± 0.014	± 0.010	± 0.009

Table 5. I-band photometric results: mean magnitude and standard deviations

	Fitting	**Clean**	**Deconv**
A	16.957 ± 0.027	16.966 ± 0.027	16.961 ± 0.025
σ_{mean}	± 0.006	± 0.006	± 0.006
B	17.170 ± 0.024	17.192 ± 0.030	17.189 ± 0.023
σ_{mean}	± 0.006	± 0.007	± 0.005
C	17.973 ± 0.054	17.910 ± 0.065	17.976 ± 0.042
σ_{mean}	± 0.013	± 0.015	± 0.010
D	18.265 ± 0.067	18.206 ± 0.083	18.242 ± 0.034
σ_{mean}	± 0.016	± 0.020	± 0.008

Fig. 2. Photometric magnitudes as a function of seeing (in arcseconds) for the B, V, R and I frames. Note that in the V-band, the magnitude of component D, derived with the Fitting method on the image with a seeing of $1\farcs63$ is outside the plot.

the errors increase when the seeing gets worse. One frame in the R-band and one in the V-band were removed from the analysis using these two methods, since they would have biased the results. We find that only the frames with a seeing better than $1\farcs1$ allow us to obtain a photometric accuracy better than 0.05 magnitudes with these two methods. The MCS algorithm is less dependent on seeing and all the frames with a seeing up to $1\farcs7$ gave photometric errors below 0.04 magnitudes. If we consider data with an integrated $S/N \sim 700$ over one point source and a seeing $FWHM \leq 1\farcs00$, the overall 1σ error bar is below 0.02 magnitudes for the A and B components and below 0.04 magnitudes for the C and D components, for all three methods. Fig. 2 presents the magnitudes for the B, V, R and I band frames respectively, measured with the three different techniques. The magnitudes are plotted as a function of seeing (in arcseconds). One of the frames with a seeing of $\sim 1\farcs48$ was discarded from the R-band figures. We notice systematic differences of the order of 0.1 magnitudes between the three methods for the C

and D components in the R-band. This is more than the standard deviations calculated on the mean values and indicates that systematic errors introduced by the analysis algorithm might significantly affect the photometry of the Einstein Cross. In several cases, a correlation between the four QSO images is observed in the frames with bad seeing values. This may be due to inaccurate scaling of the galaxy.

The results displayed in Fig. 2 have motivated photometric tests on simulated frames of the object, in order to investigate the effects of random and systematic errors on the photometry. Synthetic images were created with the three different models of the lensing galaxy (de Vaucouleurs profiles and numerical models) and with different seeing values. We found that the photometric results from the Fitting method and the CLEAN algorithm depend on both seeing and galaxy model. Implementing an accurate numerical galaxy model into the Fitting and the Clean algorithms would therefore certainly improve their efficiency and accuracy, in particular for bad seeing values. The random errors are of the same order as the statistical errors we calculated from the real frames. The systematic errors are smaller than 0.05 magnitudes for the A and B component, but up to 0.1 magnitude for the C and D components both for the Fitting method and the CLEAN algorithm when tested on the images created with different galaxy models. No systematic correlation was found between the photometry of images with different galaxy models analysed with different methods, indicating that these systematic errors are difficult to correct for.

For the deconvolution method, the systematic errors are smaller than 0.05 magnitude for all the components, and the results depend much less on the seeing of the frames since a detailed numerical galaxy model is used.

4.2. Astrometric results

The relative positions measured for the four components using the different methods are in fairly good agreement, not only with one another, but also with the positions determined from observations with the HST (Crane et al. 1991, Rix et al. 1992 and Blanton et al. 1998) and the results from the photometric monitoring published by Østensen et al. (1996). Fig. 3 presents the geometry of the object relative to component A, as derived from the three methods, and compared with previously published astrometry. Note that only the frames with a subarcsecond seeing were used for the Fitting method and the CLEAN algorithm. We found that the astrometric accuracy of these two methods significantly decreases with bad seeing. With a seeing worse than $1\farcs1$, typical errors of $0\farcs02$ are observed. The errors seem to be random with the Fitting method, whereas with the CLEAN algorithm, the positions measured for the C and D component tend to drift towards the galaxy's nucleus when the seeing gets worse.

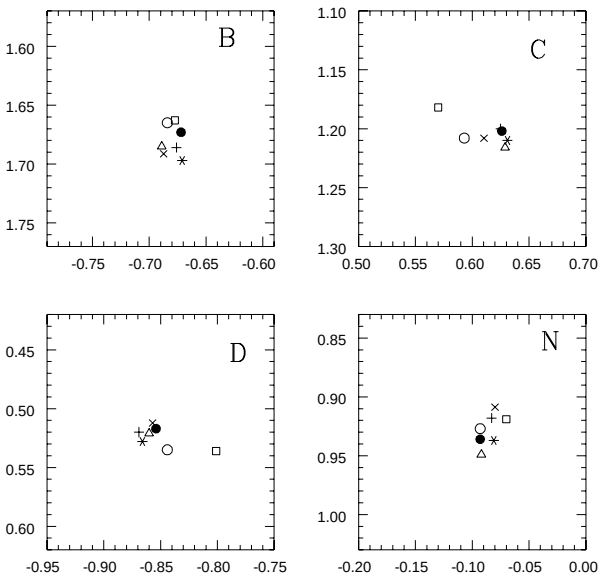

Fig. 3. Mean positions relative to the A component from all methods. The x and y axis give respectively R.A. and Declination in arcseconds relative to A. The symbols correspond to the following: × Fitting, □ CLEAN, △ MCS, • Crane et al. , + Rix et al., ∘ Østensen et al., ∗ Blanton et al.

The astrometry obtained with the deconvolution algorithm is much less seeing dependent as soon as an accurate numerical galaxy model is used. However, obtaining such a galaxy model requires the nucleus' position to be well estimated from high S/N data (see Section 3.3). This is particularly true in the B-band where the nucleus is very faint and its position less accurate (about $0\farcs05$).

5. The lensing galaxy

5.1. Morphology

As described in Section 3.3 and shown in Fig. 1, the MCS code produces a deconvolved numerical galaxy both with and without nucleus. The contour plot displayed in Fig. 4 clearly reveals a bar in the central 10 arcseconds of the galaxy. It has a very similar shape in the V and R bands whereas in the B band the S/N of the data is too low to derive an accurate galaxy profile. The bar cannot be correctly modeled by a pure analytical profile, even in the centre of the galaxy, as in fact suggested by the significant residuals obtained with the Fitting and the Clean algorithms. Photometry obtained by using only analytical models is therefore likely to be biased.

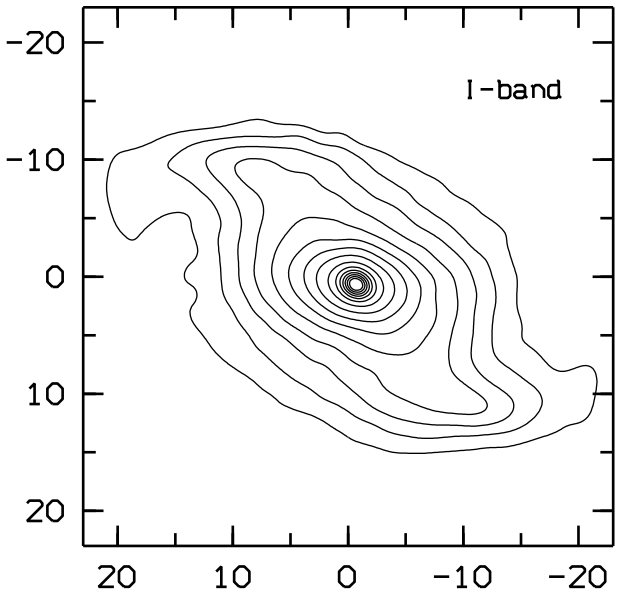

Fig. 4. Contour plots of the numerical galaxy model from the MCS deconvolution code in the I band. Both axis are in arcseconds. North is up and East is to the left.

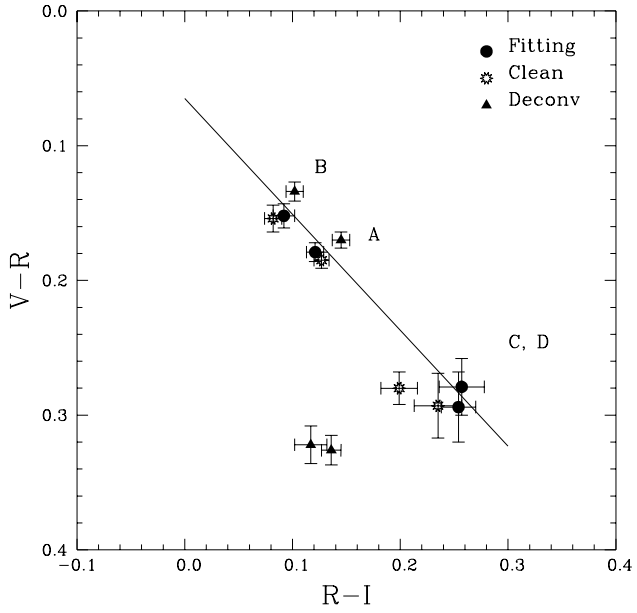

Fig. 5. V-R as function of R-I for the three different methods with error-bars on the mean of all the frames (σ_{mean} in Tables 2-5). The mean extinction law for our Galaxy is drawn as a solid line through the mean colour of the A component. See Section 5 for an explanation of the C and D points.

5.2. Extinction

From our analysis, we found that the A component is reddened relative to B, and that the C and D components are both reddened relative to A. Fig. 5 shows the $V-R$ colour as a function of $R-I$. The error-bars indicated are the errors on the mean (σ_{mean} in Tables 2-5). If the reddening is due to extinction from the galaxy, the four quasar images should lie approximately on a straight line representing the extinction law for the lens galaxy. Since it has been suggested that this law is similar to the one of our Galaxy (Yee 1988), the mean extinction law for the latter is shown on Fig. 5, as a solid line with a slope of 0.86 (Vakulik et al. 1997). Cardelli et al. (1989) showed that in the V-R-I domain, the shape of the extinction law is insensitive to the parameter $\mathrm{R_V} = \mathrm{A_V/E(B\text{-}V)}$, thus independent on the origin of the extinction (e.g., interstellar matter, dense clouds). From Fig. 5, the results from the Fitting and the CLEAN as well as the A and B magnitude from MCS could be interpreted as extinction. The positions of components C and D compared to A and B on the straight line can be explained by reddening due to the tilt of the galaxy in the direction of C and D. This tilt might even explain the reddening of A compared to B. However, we point out that the magnitudes obtained with Fitting and CLEAN in the different bands do not agree with each other, but by coincidence the differences cancel out in this particular colour plot.

Considering the differences in C and D between the three methods we can not confirm the presence of a mean extinction law. In particular, the C and D results from MCS could be interpreted as a long time colour dependent microlensing effect. When the source passes a microcaustic, its inner and hence bluer parts may be more amplified than the outer emission line region of the accretion disk. (Kayser et al. 1986 and Wambsganss & Paczyǹski, 1990). This is even true for sources angularly larger than the Einstein radius of the lens (Refsdal & Stabell 1991).

We found a colour excess of B with respect to A of $\Delta E(V-I) = -0.08 \pm 0.02$, magnitudes. This is in agreement with Vakulik et al. (1997) who found $\Delta E(V-I) = -0.12 \pm 0.05$ magnitudes, also from observations taken in 1995. However, Yee et al. (1988) found that B was reddened relative to A, $E(g-i) = +0.08 \pm 0.03$.

A possible change in the relative colours over time might be explained by colour dependent microlensing or, less likely, by dust extinction that varies over time (e.g., Rix et al. 1992). The reason for a colour change in the Einstein Cross will remain unclear unless long term multicolour photometric monitoring (or preferably spectrophotometry) is carried out on a dedicated telescope.

6. Discussion and conclusions

The two most complete light curves from photometric monitoring of the Einstein Cross have been published by Corrigan et al. (1991) and more recently by Østensen et al. (1996). Although several obvious microlensing events have been observed, no precise estimates of the photometric errors have been discussed so far. Moreover, better sampling of the light curves, as well as more accurate photometric measurements are needed in order to interpret the observed intensity differences in detail. In the present study, a set of observations in four bands was obtained during two successive nights. Since the time delay for the Einstein Cross is of the order of one day, observations on a short time scale would make it possible to separate intrinsic variations from microlensing effects.

A bright star is available on all our frames to perform PSF photometry with the three different methods considered in this paper. The seeing during the two nights was variable (0.″6-1.″7), which allowed us to quantify the seeing dependence of the different methods applied.

Differences are observed between the photometric measurements obtained with the three methods (see Fig. 2). All the methods show random errors that, as one should expect, increase with bad seeing. In addition, systematic errors in one or more of the methods are also present, especially for the fainter components of Q 2237+0305. For each QSO component, the dispersion between the mean magnitude obtained with the 3 techniques is larger than the error measured (σ_{mean}) for each method. Photometric measurements performed on simulated frames also showed that the systematic errors depend both on the seeing and on the galaxy model used to describe the deflector. The Fitting and the Clean algorithms produce large errors (0.04-0.1 magnitudes) for the two faint quasar components (C and D) when the seeing is worse than 1.″0. The errors from the MCS algorithm are below 0.04 magnitudes and less dependent on the seeing when a numerical galaxy model is used.

If only subarcsecond seeing frames are considered, we find that all three methods could have detected intensity variations with a minimum amplitude of 0.02 and 0.04 magnitudes in components A, B and C, D respectively. The latter errors are given for one individual measurement and can be improved by using several frames. When the exposures are of ∼200s, as in our case, about 10 frames can be obtained in one hour of observation. If 10 frames with a subarcsecond seeing are obtained, the random error will be $0.02/\sqrt{10} = 0.006$ and $0.04/\sqrt{10} = 0.013$ magnitudes for A, B and C, D respectively.

Assuming that systematic errors are present, it is reasonable to think that they would be more important when an analytical galaxy model is used, rather than when a purely numerical model is applied. Even if an analytical de Vaucouleurs profile can fit the central bulge of the galaxy, it cannot model the bar in the spiral galaxy, and we cannot exclude that this may affect the photometry of the quasar images. Moreover, a good numerical model obtained from high S/N data can represent high frequency structures in the galaxy which would be neglected by an analytical model. For example, H II regions in the lens galaxy can only be modeled by a numerical profile. Such clumpy structures, likely to emit in the H_α line, would then make inaccurate the R-band photometry obtained with any analytical galaxy model. In such a case, the photometry of the C and D components would be most affected since their positions are along the bar of the galaxy, where most of the H II regions should lie. The largest photometric differences between the methods investigated here are indeed present in the R-band, but H_α-imaging would be needed to confirm such an effect by directly imaging the H II clumps. We should also point out that finding a numerical galaxy involves a larger number of free parameters. In the present case, we cannot rule out the possibility that the S/N in our frames was too low to obtain a unique numerical model.

Based on the published light curves and the present study, we propose the following observational strategy for a future photometric monitoring of the Einstein Cross. The aimed sampling of the points on a light curve should be compared with typical time scales of microlensing events. Since time scales as short as 14 days have been observed (Østensen et al. 1996), a sampling of the order of a few observations per night should be aimed at. Furthermore, since intensity variations of 0.05 magnitudes or less can be expected (Østensen et al. 1996), it is important to ensure a photometric accuracy well below this value. As shown in our study, using several data frames (up to 10 with a 2m class telescope) to derive any individual photometric measurement would yield random error bars smaller than 0.01 magnitude for subarcsecond observing conditions, and would allow such a monitoring program.

However, one cannot expect subarcsecond conditions over observing runs as long as several nights. Given this observational constraint, it is likely that the best photometric accuracy will be obtained by using a detailed numerical galaxy model. We have shown that such a galaxy model can be constructed from high S/N frames with the MCS algorithm and that accurate photometry can be achieved by applying this model in connection with simultaneous deconvolution of all the frames.

Acknowledgements. We wish to thank S. Sohy for help with the MCS algorithm, and J.P. Swings for support. IB, FC, and RØ are supported in part by contract ARC94/99-178 "Action de Recherche Concertée de la Communauté Française (Belgium)" and Pôle d'Attraction Interuniversitaire, P4/05 (SSTC, Belgium).

References

Blanton, M., Turner, E.L., Wambsganss, J., 1998, preprint astro-ph/9805359

Cardelli, J.A., Clayton, G.C., Mathis, J.S., 1989, ApJ, 345, 245

Chang, K., Refsdal, S., 1979, Nature, 282, 561
Corrigan, R.T., Irwin, M.J., Arnaud, J., et al., 1991, AJ, 102, 34
Courbin, F., Lidman, C., Magain, P., 1998a, A&A, 330, 57
Courbin, F., Lidman, C., Frye, B., et al. 1998b, ApJ, 499, L119
Crane, P., Albrecht, R., Barbieri, C., et al. 1991, ApJ, 369, L59
Huchra, J., Gorenstein, M., Kent, S., et al., 1985, AJ, 90, 691
Kayser, R., Refsdal, S., Stabell, R., 1986, A&A, 166, 36
Kayser, R., Refsdal, S., 1989, Nature, 338, 745
Magain, P., Courbin, F., Sohy, S., 1998, ApJ, 494, 472
Østensen, R., 1994, Cand. Scient. Thesis, University of Tromsø
Østensen, R., Refsdal, S., Stabell, R., et al., 1996, A&A, 309, 59
Østensen, R., Remy, M., Lindblad, P.O., et al., 1997, A&AS, 126, 393
Paczyǹski, B., 1986, ApJ, 301, 503
Press, W.H., Flannery, B.P., Teukolsky, S.A., & Vetterling, W.T., 1989, Numerical Recipes (Cambridge: Cambridge Univ. Press)
Refsdal, S., Stabell, R., 1991, A&A, 250, 62
Remy, M., 1996, Ph.D. Thesis, Liège University
Rix, H.-W., Schneider, D.P., Bahcall, J.N., 1992, AJ, 104, 959
Stetson, P.B., 1987, PASP, 99, 191
Teuber, J., 1993, Digital Image Processing, Prentice-Hall
Yee, H.K.C. 1988, AJ, 95, 1331
Vakulik, V.G., et al., 1997, Astron. Nachr., 318, 2, 73
Wambsganss, J., Schneider, P., Paczyǹski, B., 1990, ApJ, 358, L33